UDC 539.4

Experimental and Numerical Simulation of the Microcrack Coalescence Mechanism in Rock-Like Materials

H. Haeri,[a,1] A. Khaloo,[b] and M. F. Marji[c]

[a] Department of Civil Engineering, Sharif University of Technology, Tehran, Iran

[b] Center of Excellence in Structure and Earthquake Engineering, Sharif University of Technology, Tehran, Iran

[c] Faculty of Mining and Metallurgy, Institution of Engineering, Yazd University, Yazd, Iran

[1] haerihadi@gmail.com

УДК 539.4

Экспериментальное и численное моделирование механизма слияния трещин в материалах типа скальных пород

Х. Хаэри, А. Халу, М. Ф. Марджи

[а] Факультет гражданского строительства, Технологический университет Шариф, Тегеран, Иран

[б] Центр качества сооружений и инженерной сейсмологии, Технологический университет Шариф, Тегеран, Иран

[в] Факультет горного дела и металлургии, Университет г. Йезд, Иран

Скальные породы и скалоподобные материалы часто разрушаются при сжатии вследствие инициирования, распространения и слияния ранее возникших микротрещин. Выполнены экспериментальные и численные исследования механизма процесса слияния микротрещин в материалах типа скальных пород. Экспериментальные исследования включают в себя испытания на одноосное сжатие образцов, изготовленных из смеси цемента марки портланд пуццолан, слюды и воды. Слияние микротрещин изучается на тонких образцах с помощью сканирующего электронного микроскопа. Предполагается, что вкрапления слюды играют роль микротрещин в образцах. Также проведены некоторые аналитические и численные исследования для моделирования экспериментально наблюдаемого явления слияния микротрещин в образцах. Для оценки коэффициентов интенсивности напряжений по моде I и II в вершинах микротрещин используется косвенный метод граничных элементов высокого порядка, известный как метод разрыва перемещений высокого порядка, что позволяет применять специальные элементы у вершины трещины для учета сингулярности полей напряжений и перемещений вблизи вершины трещины. В программе расчета напряжений используется критерий разрушения по максимальным касательным напряжениям в рамках линейной механики разрушения. При этом распространение и слияние микротрещин, распределенных в скальной породе по случайному закону, оценивалось путем численного моделирования на основе итеративного алгоритма. Полученные расчетные результаты сравниваются с соответствующими экспериментальными и численными данными по слиянию микротрещин в скалоподобных материалах.

Ключевые слова: слияние микротрещин, коэффициенты интенсивности напряжений, численное и экспериментальное моделирование, метод разрыва перемещений высокого порядка, скалоподобные материалы.

© H. HAERI, A. KHALOO, M. F. MARJI, 2015

Introduction. Microcracks may be considered as the main defects in rocks and rock materials. Microcracks usually initiate, propagate and coalesce to produce the macrocracks, which are responsible for the final breaking of brittle solids. One of the most challenging problems in fracture mechanics is simulation of the failure mechanism and crack propagation process in brittle solids such as rocks [1–4]. The mechanism of crack propagation in solid materials can be investigated in micro- and macroscales, which deal with initiation and propagation of microcracks and bigger cracks, respectively.

The presence of microcracks in solids is the most effective issue pertaining to the mechanical behavior of brittle materials. It can be found to what extent macrofracturing mechanism is effected by microfracturing mechanism [5–8].

The mechanical behavior of rocks as the brittle materials also depends on their micromechanical structure [9]. The microcracks typically nucleate at the pores, inclusions, sharp microcracks, and triple connections where the stress concentration may occur. The creation and propagation of microcracks play an important role in predicting the cyclic breakage process of rocks [10]. The pre-existing microcracks can propagate and extend to form macrocracks [11]. These macrocracks may be further propagated to form the kinked or curved cracks containing wing and secondary cracks [12, 13]). The breakage mechanism of brittle solids with randomly orientated microcracks depends on the degree of micro-cracks interacting and their coalescence path which may finally leads to a crack in macroscale. In the failure process of brittle rocks (under uniaxial compression), two types of cracks may be observed which are originating from the tips of the pre-existing microcracks (i.e., wing cracks and secondary cracks as shown in Fig. 1).

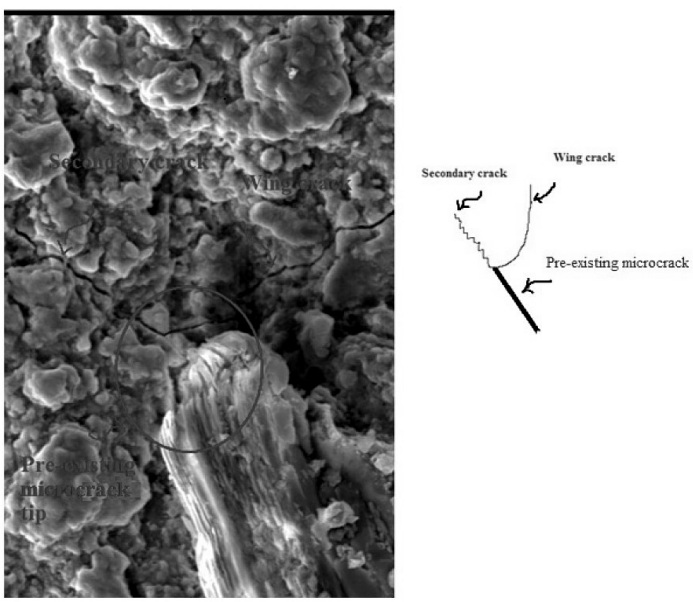

Fig. 1. Wing and secondary cracks observed near the tip of a pre-existing microcrack.

Wing cracks may generally initiate at or near the tips of the pre-existing microcracks and continue their propagation in a curved form path. The secondary cracks may also nucleate from the tips of the pre-existing cracks simultaneously or after the wing cracks nucleation and propagation. [14–17].

Compression tests are of versatile use to perform most experiments on various types of polycrystalline solids such as geomaterials [14–24]. For example, Cheng-zhi and Ping [25] have conducted some compression tests on rock-like specimens containing closed

multi-fissures. The influence of natural flaws inclination angles and the fissures distribution density on the breakage mechanism of fractured bodies have been studied in their research work.

Many numerical methods such as finite element method (FEM), boundary element method (BEM), discrete element method (DEM), and displacement discontinuity method (DDM) have been developed in the literature which can be effectively used for the simulation of microcracks initiation and propagation in geomaterials.

The geomaterials such as rocks and concretes are behaving elastically and in a brittle manner so that the concept of linear elastic fracture mechanics (LEFM) proposed by Irwin [26] may be suitable to study the mechanism of microcracks propagation and coalescence in these solid substances. Based on LEFM suggestion, the three modes of stress intensity factors, K_{I} (mode I or opening mode), K_{II} (mode II or shearing mode), and K_{III} (mode III or tearing mode), are being used for crack analysis of brittle materials [26]. Basically, the three classic fracture criteria; maximum tangential stress criterion (σ-criterion), the minimum energy density criterion (S-criterion) and the maximum energy release rate criterion (G-criterion) or any modified form of these criteria (e.g., F-criterion which is a modified energy release rate criterion) have been used to study the crack initiation and propagation under mixed mode I–II loading conditions (which are the most applicable in rock fracture mechanics) [27–30]. In most cases either of these three fracture criteria can be suitably used for fracture analysis of rocks and rock-like materials [31].

Numerical or analytical approaches are mostly used to investigate the rock breakage mechanism due to complexity of the fracture mechanics problems in brittle materials [32]. In this study, a comprehensive analytical, numerical and experimental approach is developed to analyze the crack propagation in rocks and rock-like materials under uniaxial compressive loading. A typical analytical study is presented first, and then several compression tests on cylindrical specimens of rock-like materials containing microcracks are performed. The rock-like specimens prepared from PCC, mica sheets (to represent the random microcracks) and water. These specimens are tested under uniaxial compression in a concrete laboratory. The same experiments are also simulated numerically by a modified higher-order displacement discontinuity method where the microcracks' propagation mechanism are studied based on Mode I and Mode II SIFs and maximum tangential stress (MTS) criterion. In this research a modified indirect boundary element method based on the cubic variations of displacement discontinuities along a straight line microcrack is developed to implement the special crack tip elements and evaluate the Mode I and Mode II SIFs. A sophisticated computer code is prepared using a higher-order displacement discontinuity variation with three equal subelements near each crack end.

The well-known scanning electron microscopy (SEM) technique is used for a direct observation of microcracks, their propagation paths and coalescence. By comparing the SEM results of microcrack propagation paths with those numerically predicted, the proposed numerical method allows one to validate the present microcrack analyses of rock-like materials.

1. **A Center Slant Crack in an Infinite Body**. A center slant crack is considered in an infinite body with a half-length $b = 5$ mm and inclination angle φ changing counterclockwise from the y axis, and the compressive stress σ is acting parallel to the y axis (as shown in Fig. 2). The analytical solution of this typical fracture mechanics problem is given in the literature [19].

Based on the configuration shown in Fig. 2, the analytical solution for Mode I (K_{I}) and Mode II (K_{II}) SIFs in an infinite body containing a center slant crack can be estimated as

$$\begin{aligned} K_{\mathrm{I}} &= -\sigma\sqrt{\pi b}\,\varpi_{\mathrm{I}}, \\ K_{\mathrm{II}} &= -\sigma\sqrt{\pi b}\,\varpi_{\mathrm{II}}, \end{aligned} \tag{1}$$

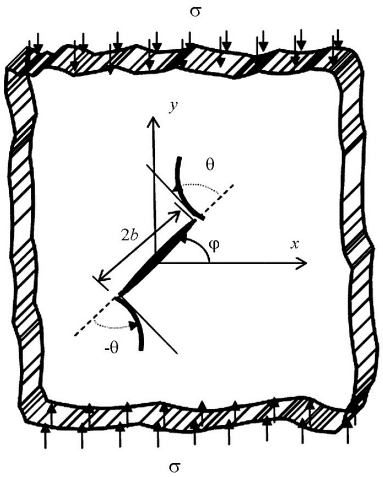

Fig. 2

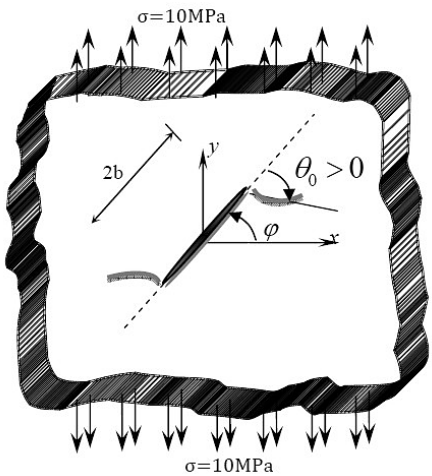

Fig. 3

Fig. 2. A center slant crack in an infinite plane under uniaxial compression.
Fig. 3. A center slant microcrack in an infinite body under uniform tension parallel to the y axis.

where σ (in MPa) is the compressive stress at the crack initiation state, b (in mm) is half of the crack length, and ϖ_{I} and ϖ_{II} are the non-dimensional coefficients (depending on the crack inclination angle φ) which can be expressed as

$$\varpi_{\mathrm{I}} = \frac{1+\cos 2\varphi}{2}, \qquad \varpi_{\mathrm{II}} = \frac{\sin 2\varphi}{2}. \tag{2}$$

Equations (1) and (2) give the SIFs at the microcrack tips which are affected by the crack geometry such as the microcrack length b and the microcrack inclination angle φ.

The center slant crack problem in an infinite body under uniform tension (Fig. 3) has also been solved by different researchers, e.g., Guo et al. [43] (to compare the accuracy of different crack analyses).

Most of the previous researchers used the constant element displacement discontinuity with a special crack tip element but considered different crack inclination angles (e.g., $\varphi = 30$, 40, 50, 60, 70, and 80°). To evaluate the microcrack initiation angle θ_0, the maximum tangential stress criterion (σ_θ-criterion), is being used in this microcrack analysis. Table 1 compares the results of this analysis (using the two dimensional higher-order displacement discontinuity method (HDDM^{2D} Code) with the results of other models cited in the literature. As it can be seen in Table 1, the numerical results obtained by HDDM^{2D} Code are comparatively more accurate.

2. **Experiments Performed on Rock-Like Materials with Random Microcracks**. A conventional compressive test apparatus in a concrete or rock mechanics laboratory can be used to test the specimens of rock-like material. These specimens are the specially prepared samples from portland pozzolana cement (PPC), water and mica sheets. A typical specimen is shown in Fig. 4. The mica sheets are approximately 5 mm in size and simulate the number of random pre-existing microcracks within the rock-like specimens. In this research, a cylindrical specimen with a height to diameter ratio of 1 (the diameter and length of the specimens are both equal to 54 mm) is being provided and tested under uniaxial compression in the laboratory. The ingradients' mixing ratios and the mechanical

T a b l e 1

Microcrack Initiation Angle θ_0 for a Center Slant Microcrack Problem Obtained by Different Methods

Crack inclination angles φ, deg	θ_0, deg			
	Results obtained by HDDM^{2D} code	Results obtained by Guo et al. [35, 36]		
	Cubic elements	S-criterion	Experimental	Numerical
30	62.01	63.5	62.4	67.0
40	55.65	56.7	55.1	59.0
50	51.29	49.5	51.1	51.0
60	43.22	41.9	43.1	41.0
70	30.26	31.8	30.7	29.0
80	17.91	18.5	17.3	15.0

T a b l e 2

Ratio of Ingredients and Mechanical Characteristics of Rock-Like Specimen

Ingredients' ratio (%)			Mechanical properties				
PPC	Mica sheets	Water	Tensile strength (MPa)	Uniaxial compression strength (MPa)	Fracture toughness (MPa · m$^{1/2}$)	Elastic modulus (GPa)	Poisson's ratio
50.5	5.0	44.5	1.5	3.7	2.0	5.0	0.17

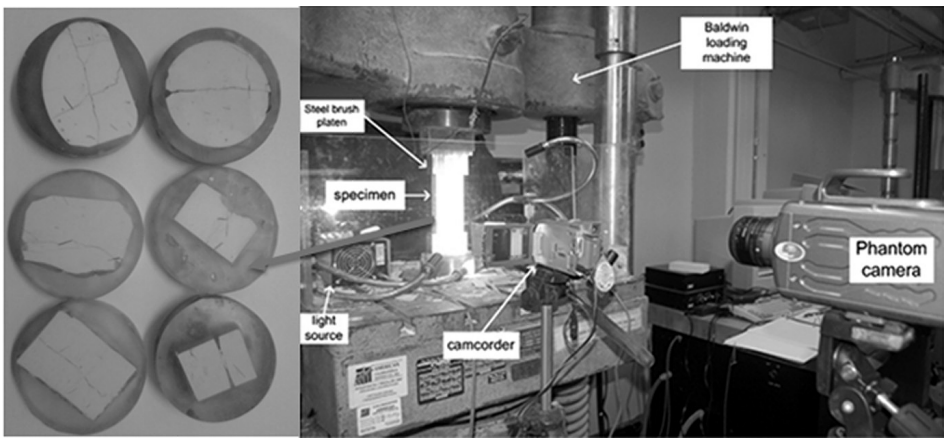

Fig. 4. Experimental set up for uniaxial compression test containing microcracks and the polished sections used for SEM study.

properties of the rock-like specimens were obtained from the experimental tests performed in the laboratory and presented in Table 2. All the tests were performed based on ISRM suggested methods [33, 34]. Then, the polished sections are specially prepared as shown in Fig. 4. The initiation and propagation of microcracks in the rock-like specimens (containing random microcracks) are studied by SEM.

In the present analysis, a novel effective method is developed to investigate the wing crack initiation and propagation (nucleating from the original microcrack tips). The

polished sections involving random microcracks are specially prepared and studied under SEM. In preparing the polished sections, it is tried to preserve the breakage surface, therefore, the polished sections are taken from the central part of the loaded specimens and are then soaked into a mixture of resin, cobalt oxide and HCL. Some good images are prepared to visualize the microcracks propagation paths and their coalescence phenomena during the fracturing process of the rock materials samples.

3. **Experimental Results**. Two types of emanating cracks form the tips of the pre-existing microcracks in brittle materials may be produced under uniaxial compressive loading conditions. The primary wing cracks usually produced due to induced tensile stresses near the crack ends and secondary cracks (oblique and/or coplanar) which may be produced due to shear stresses along the crack surfaces. The propagating wing cracks are expected to extend parallel to the direction of maximum compression.

In a crack propagation process, the secondary cracks may not always appear but the wing cracks are suddenly appear at the starting point of microcrack growth. These propagating wing cracks may also further extend to coalesce with the other nearby microcracks, and forming the final macrocracks. The macrocracks (or bigger cracks) may propagate and coalesce with other microcracks or cracks to cause the final breakage of the material.

In this research, a series of uniaxial compression tests are carried out on rock-like specimens, and the propagation direction of microcracks are determined. Some of the experimentally observed wing and secondary cracks at the tips of the microcracks are shown in Figs. 5–8, respectively. It is experimentally observed that the wing cracks occur when the microcrack inclination angle φ (with respect to the loading direction) is between 30 and 80°. The wing cracks may not occur when the pre-existing microcrack angle is less than 30°. However, it may be deduced that the wing cracks initiation angles ranged between 30 and 70° with respect to the direction of the pre-existing microcracks.

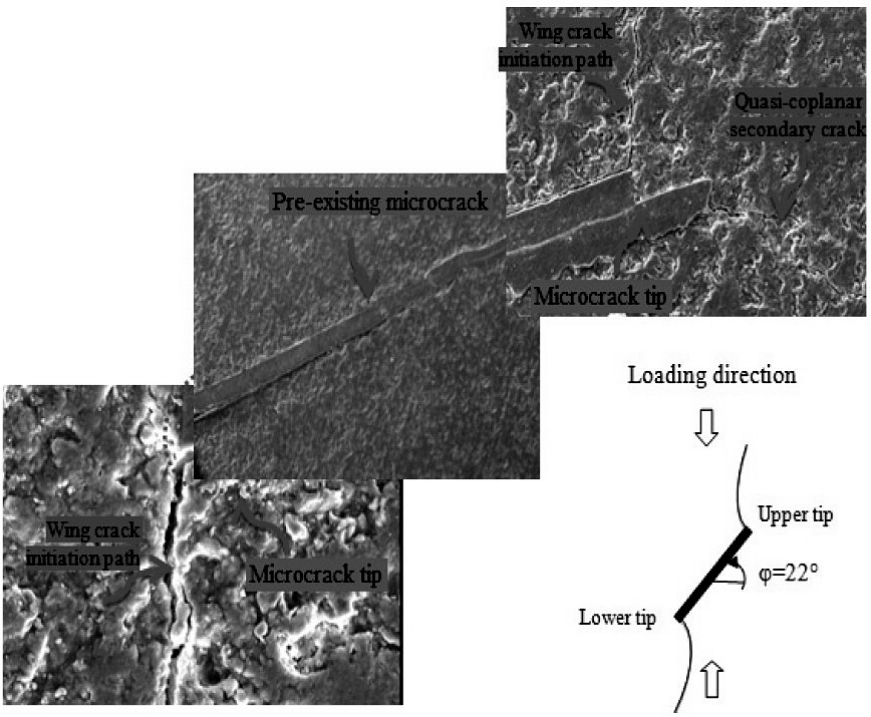

Fig. 5. Wing cracks observed near the two tips of a pre-existing microcrack in rock-like specimens under uniaxial compression ($\varphi = 22°$).

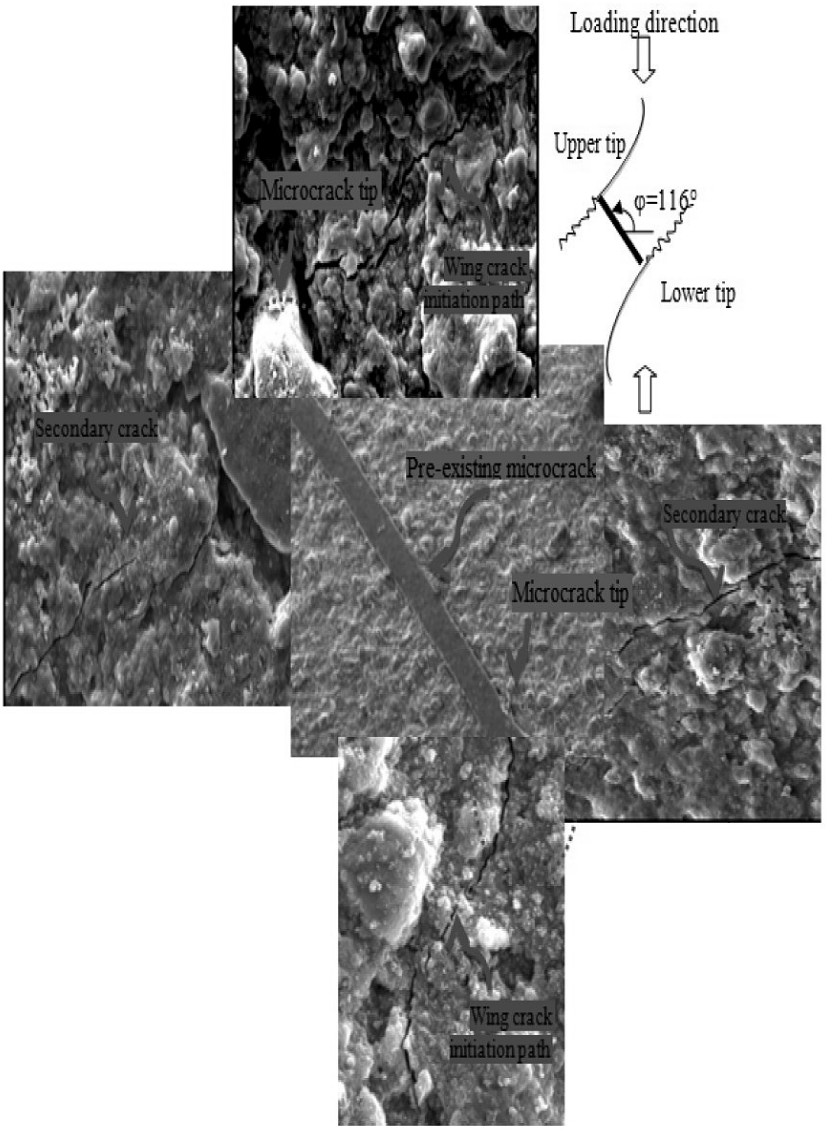

Fig. 6. Wing and secondary cracks observed near the two tips of a pre-existing microcrack in rock-like specimens under uniaxial compression ($\varphi = 116°$).

As shown in Fig. 5, wing cracks initiate at both tips of a microcrack. However, secondary crack may initiate only at the upper tip of a microcrack. In Fig. 6, wing and secondary cracks initiate at the same time from the two tips of a microcrack. In Figs. 7 and 8, only the wing cracks are observed and the secondary cracks do not exist.

The rock-like specimens (made from cement, mica sheets and water) have a lower strength compared to that of natural rocks (such as granite or marble). Due to much lower strength of mica sheets compared to that of the matrix of the prepared specimens, the mica sheets are considered to play the role of microcracks within the rock-like samples. The experimental results obtained by testing such samples are studied by SEM and the propagation angles and paths of the microcracks are traced. These observations are in good agreement with the numerical results obtained by the numerical simulations (as explained in the next section).

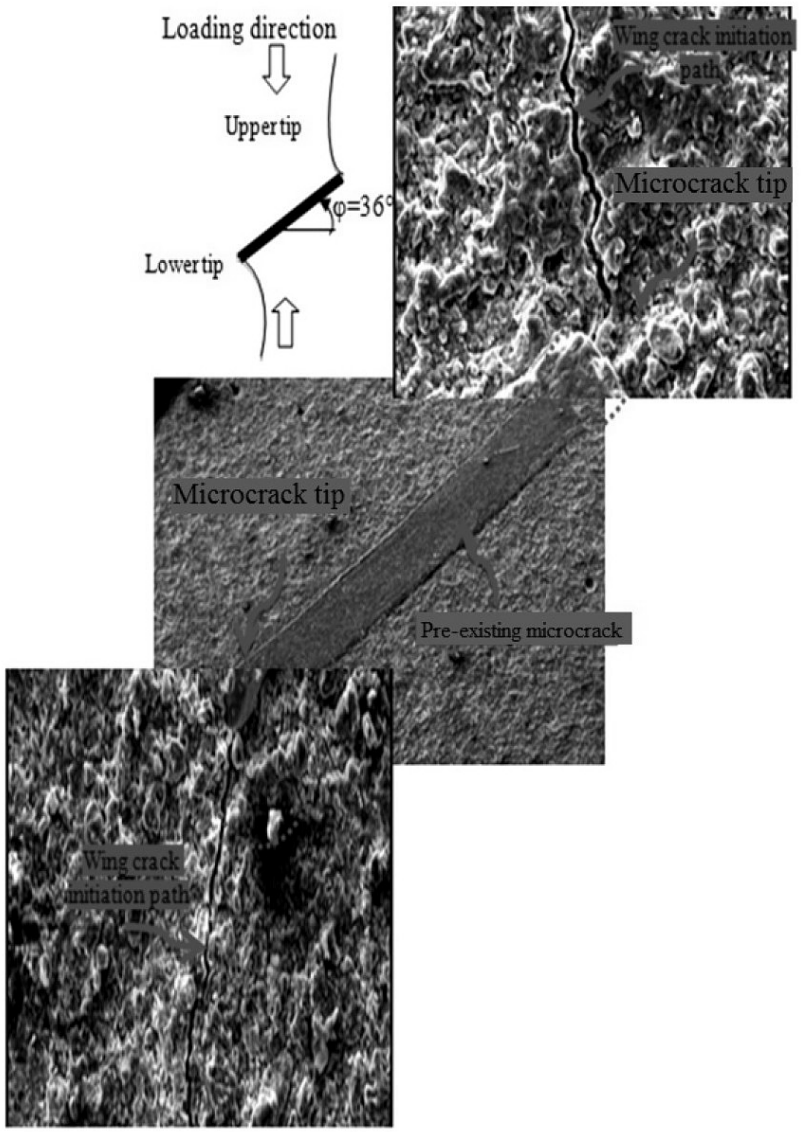

Fig. 7. Wing and secondary cracks observed near the two tips of a pre-existing microcrack in rock-like specimens under uniaxial compression ($\varphi = 36°$).

4. **Numerical Study of Propagation and Coalescence of Random Microcracks**. The experimental tests can be used to visualize the microcracks propagation and coalescence and also they can be used to validate the proposed numerical simulation developed in this study for the investigation of rock breakage mechanism due to the propagation of pre-existing microcracks in rock-like materials. The specimens (representing rock-like specimen), are made of PPC, water and mica sheets and are tested as explained in the previous section. In this section, a higher-order displacement discontinuity method is proposed to simulate the microcrack propagation mechanism in rock-like specimens.

4.1. ***The Higher-Order Displacement Discontinuity Method***. The higher-order displacement discontinuity method (DDM) is a category of the indirect boundary element method used for solving the linear elastic problems with specified boundary conditions. A third-order variation of continuous stress and discontinuous displacement fields at the

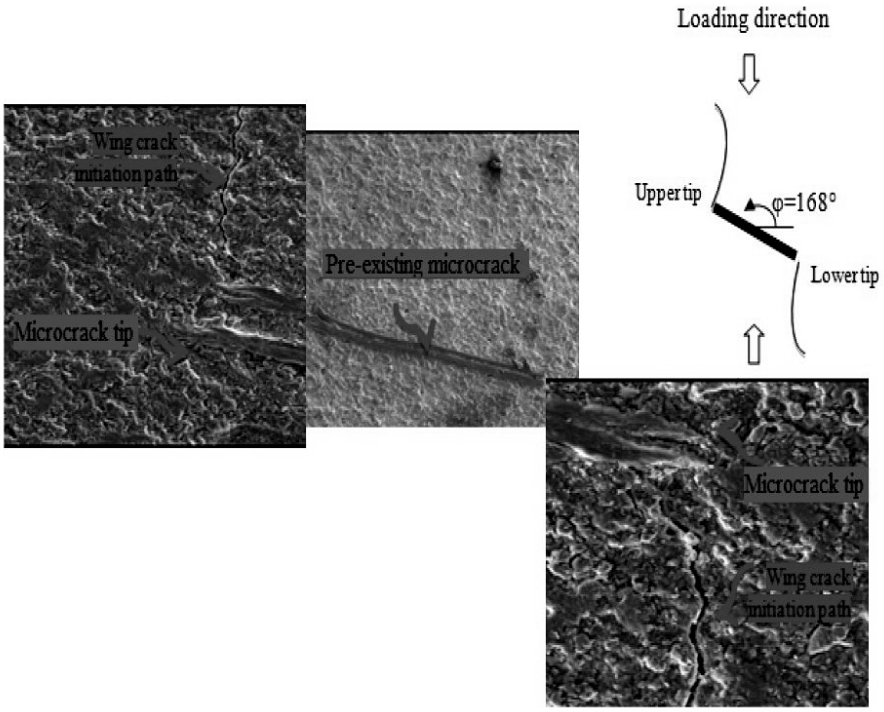

Fig. 8. Wing cracks observed near the two tips of a pre-existing microcrack in rock-like specimens under uniaxial compression ($\varphi = 168°$).

boundaries (discretized into a proper number of line crack elements) is assumed [35–40]. In the present study, a two-dimensional higher-order displacement discontinuity method ($HDDM^{2D}$) employing the cubic displacement discontinuity (DD) elements (third-order DD discontinuity elements) in order to obtain more accurate displacement discontinuities along the boundary of the problem. In a cubic displacement discontinuity (DD) variation each source element is divided into four equal subelements. Each subelement contains a central node where the nodal displacement discontinuities are numerically evaluated. Based on this variation of DD, the displacement discontinuity $D_j(\varepsilon)$ for each cubic element can be formulated as

$$D_j(\varepsilon) = \sum_{i=1}^{4} \Pi_i(\varepsilon) D_j^i, \qquad j = x,\ y, \tag{3}$$

where D_x^1, D_y^1, D_x^2, D_y^2, D_x^3, D_y^3, D_x^4, and D_y^4 are the cubic nodal displacement discontinuities and the collocation shape functions $\Pi_i(\varepsilon)$ can be expressed as

$$\begin{aligned}
\Pi_1(\varepsilon) &= -(3a_1^3 - a_1^2\varepsilon - 3a_1\varepsilon^2 + \varepsilon^3)/(48a_1^3),\\
\Pi_2(\varepsilon) &= (9a_1^3 - 9a_1^2\varepsilon - a_1\varepsilon^2 - \varepsilon^3)/(16a_1^3),\\
\Pi_3(\varepsilon) &= (9a_1^3 + 9a_1^2\varepsilon - a_1\varepsilon^2 - \varepsilon^3)/(16a_1^3),\\
\Pi_4(\varepsilon) &= -(3a_1^3 + a_1^2\varepsilon - 3a_1\varepsilon^2 - \varepsilon^3)/(48a_1^3).
\end{aligned} \tag{4}$$

Here $a_1 = a_2 = a_3 = a_4$. It should be noted that a cubic element has 4 nodes, which are located at the centers of its four subelements as shown in Fig. 9.

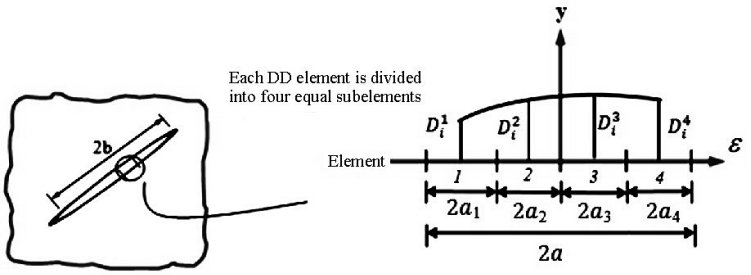

Fig. 9. The cubic collocation technique used in the higher-order displacement discontinuity method.

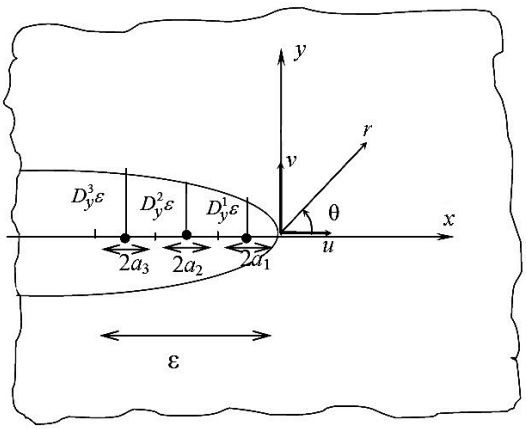

Fig. 10. A special crack tip element with three equal subelements for a right crack tip.

As shown in Fig. 9, a cubic displacement discontinuity (CDD) element is divided into four equal subelements (each subelement contains a central node for which the nodal displacement discontinuities are numerically evaluated).

The singularities of the stresses and displacements near the crack ends may reduce the accuracy of the displacement discontinuities at the nodal points near the crack tips, special crack tip elements can be used to overcome this problem and increase the accuracy of the DDs near the crack tips [40]. As shown in Fig. 10, a DD variation for three nodes can be formulated using a special crack tip element containing three nodes (or having three special crack tip subelements). Then the displacement discontinuity function $D_j(\varepsilon)$ can be defined as

$$D_j(\varepsilon)=[\Gamma_{C1}(\varepsilon)]D_j^1(a)+[\Gamma_{C2}(\varepsilon)]D_j^2(a)+[\Gamma_{C3}(\varepsilon)]D_j^3(a), \tag{5}$$

where the crack tip element has a length $a=a_1=a_2=a_3$.

Considering a crack tip element with the three equal subelements ($a_1=a_2=a_3$), the special shape functions $\Gamma_{C1}(\varepsilon)$, $\Gamma_{C2}(\varepsilon)$, and $\Gamma_{C3}(\varepsilon)$ can be obtained as

$$\begin{aligned}
\Gamma_{C1}(\varepsilon)&=\frac{15\varepsilon^{1/2}}{8a_1^{1/2}}-\frac{\varepsilon^{3/2}}{a_1^{3/2}}+\frac{\varepsilon^{5/2}}{8a_1^{5/2}},\\
\Gamma_{C2}(\varepsilon)&=\frac{-5\varepsilon^{1/2}}{8a_1^{1/2}}+\frac{3\varepsilon^{3/2}}{2\sqrt{3}\,a_1^{3/2}}-\frac{\varepsilon^{5/2}}{4\sqrt{3}\,a_1^{5/2}},\\
\Gamma_{C3}(\varepsilon)&=\frac{3\varepsilon^{1/2}}{8\sqrt{5}\,a_1^{1/2}}-\frac{\varepsilon^{3/2}}{2\sqrt{5}\,a_1^{3/2}}+\frac{\varepsilon^{5/2}}{8\sqrt{5}\,a_1^{5/2}}.
\end{aligned} \tag{6}$$

T a b l e 3

Mechanical Properties of a Center Slant Microcrack in an Infinite Plate

Description	Parameter	Value	Unit
Microcrack length	b	10	mm
Compressive stress	σ	10	MPa
Elastic modulus	E	10	GPa
Poisson's ratio	ν	0.2	–
Fracture toughness	K_{Ic}	2	$\mathrm{MPa}\cdot\mathrm{m}^{1/2}$
Microcrack tip length	L	–	mm
Microcrack inclination angle	φ	–	deg

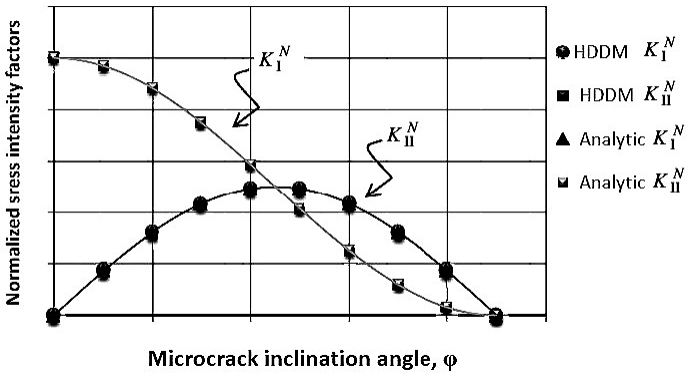

Fig. 11. The analytical and numerical values of K_{I}^N and K_{II}^N for the center slant microcrack.

4.2. ***Numerical Simulation of the Pre-Cracked Specimens***. A center slant microcrack in an infinite body under uniaxial compression (Fig. 2) is simulated numerically by the higher-order displacement discontinuity method. The numerical results are compared with the corresponding analytical results already given in Section 2 of this study. This test problem provides a better knowledge of the crack propagation mechanism and failure of the brittle materials such as rocks. It also provides a good opportunity to verify the numerical and analytical values of the mixed mode SIFs K_{I} and K_{II} for a typical problem. The mechanical properties of a rock specimen (assuming to have a slant center crack in an infinite plane) are given in Table 3. Assuming a LEFM concept [41], the Mode I and Mode II stress intensity factors K_{I} and K_{II}, for different crack inclination angles are evaluated numerically by means of the proposed numerical method [these results can also be estimated analytically using Eqs. (1) and (2) given in Section 2]. The normalized Mode I and Mode II SIFs are simplified as

$$K_{\mathrm{I}}^N = \frac{K_{\mathrm{I}}}{\sigma\sqrt{\pi b}}, \qquad K_{\mathrm{II}}^N = \frac{K_{\mathrm{II}}}{\sigma\sqrt{\pi b}}. \tag{7}$$

The numerical and analytical results of the normalized SIFs K_{I}^N and K_{II}^N are shown in Fig. 11, which illustrates the accuracy and usefulness of the proposed method for the

crack analysis of brittle solids. In the numerical analysis of this problem, 7 cubic elements have been used along the pre-existing crack, three special crack tip elements have been used for each crack tip and the ratio of crack tip element length ($L/b = 0.1$).

The validity of the proposed numerical method and the accuracy of the numerical results are checked by comparing the computed wing crack initiation directions with their corresponding experimental results given in Section 4. The wing crack initiation directions obtained from the numerical simulation and laboratory experiments by considering various microcrack inclination angles and microcrack sizes are tabulated in Table 4 for comparison. This table clearly shows that the numerical results are in good agreement with the experimental results.

T a b l e 4

The Microcrack Initiation Angle θ for the Center Slant Microcrack Problem as Obtained by the Proposed Numerical and Experimental Methods

Type of microcracks as shown in Figs. 5–8	Microcrack size (mm)	Microcrack inclination angle φ, deg	Wing crack initiation direction θ, deg			
			Numerical		Experimental	
			Upper tip	Lower tip	Upper tip	Lower tip
Fig. 5	3.5	22	67	60	66	66
Fig. 6	4.2	116	72	58	71	58
Fig. 7	3.9	36	50	45	51	51
Fig. 8	4.3	168	82	80	83	83

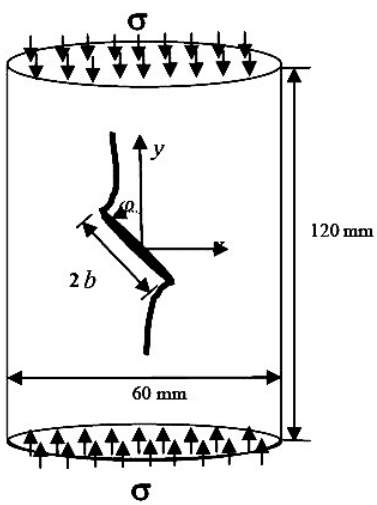

Fig. 12. A center slant crack in a finite plate.

5. **Discussion**. The experimental and numerical results given in this research are in good agreement with those already given in literature. The following discussion verifies the validity and accuracy of the present study.

Figure 12 schematically shows a rock-like specimen with length $L = 120$ mm and width $w = 60$ mm ($L/w = 2$) containing a center slant crack with a half-length $b = 5$ mm and inclination angle φ changing counterclockwise from the x axis [24]. A uniform uniaxial compressive stress is assumed to be applied parallel to the y axis of the specimen.

In order to be able to compare the numerical results of the proposed problem with those already given in the literature, the mechanical properties of the numerical model are taken the same as those given by Lee and Jeon [24] for PMMA specimens that are presented in Table 5. Lee and Jeon [24] conducted experimental tests on PMMA specimens with single pre-existing crack as shown schematically in Fig. 13. The crack propagation path is mainly due to the wing cracks produced at the crack tips which propagate in direction of the uniaxial compressive stress. In the present study, the problem shown in Fig. 12 is simulated numerically and the results are compared with those obtained recently by Lee and Jeon [24].

T a b l e 5

Mechanical Properties of a PMMA Specimen [24]

Description	Parameter	Value	Unit
Crack length	$2b$	10	mm
Compressive stress	σ	139	MPa
Elastic modulus	E	2.9	GPa
Poisson's ratio	ν	0.44	–
Fracture toughness	K_{Ic}	1.7	$\text{MPa} \cdot \text{m}^{1/2}$

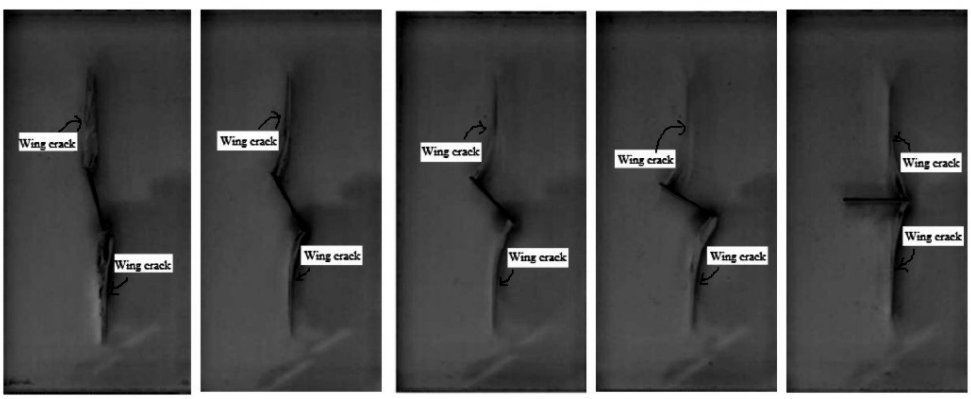

$\varphi = 15°$ $\varphi = 30°$ $\varphi = 45°$ $\varphi = 60°$ $\varphi = 90°$

Fig. 13. The crack propagation path of a single crack in the PMMA specimens with different crack inclination angles $\varphi = 15$, 30, 45, 60, and 90° [24].

In the numerical verification of the results, the typical rock-like specimen is the PMMA with mode I fracture toughness $K_{Ic} = 1.7$ $\text{MPa} \cdot \text{m}^{1/2}$ which is estimated based on the experimental results given by Lee and Jeon [24]. It should be noted that different incremental propagation steps are used in the numerical analysis of the present problem.

The experimental [24] and numerical results of crack propagation path in specimens containing single cracks with varying inclination angles $\varphi = 15$, 30, 45, 60, and 90° are shown in Figs. 13 and 14 for comparison.

Conclusions. The mechanism of microcrack propagation in brittle rocks is investigated by analytical, experimental, and numerical methods. Further work is devoted to investigate the crack propagation, cracks coalescence and crack propagation paths of the rocks and rock-like materials under compressive loading condition. The microcrack propagation in natural rocks is very complicated; therefore, some rock-like specimens are

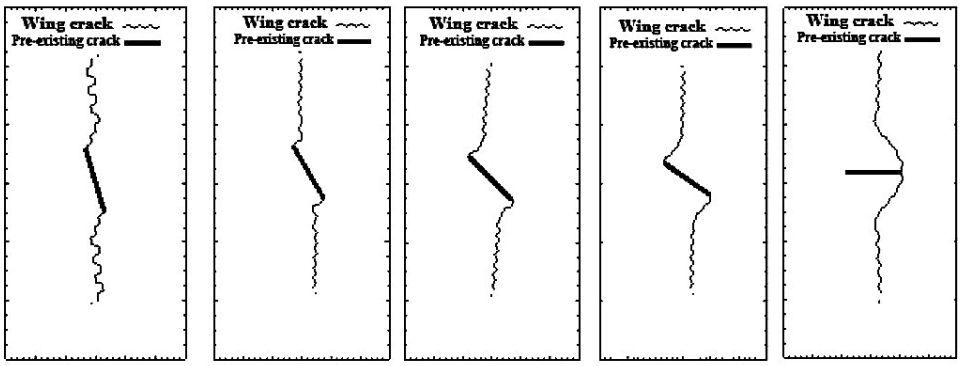

Fig. 14. Numerical simulation of the propagating paths for a single crack with variable crack inclination angles $\varphi = 15$, 30, 45, 60, and 90°.

prepared by mixing PPC, mica sheets and water. These specimens are tested under uniaxial compression and the propagation and coalescence of random microcracks (mica sheets play the role of microcracks within the specimen) are observed by SEM.

Based on the LEFM concept, the Mode I and Mode II stress intensity factors near the microcrack ends are computed analytically and numerically. The maximum tangential stress criterion (σ-criterion) is used here to investigate the microcracks initiation and their propagation directions. This criterion is implemented in the higher-order displacement discontinuity (HDD) method by a computer code named as HDDM^{2D} (i.e., a two-dimensional HDD method for microcrack analysis).

In the present analysis, the direction of wing crack initiation is numerically predicted and is compared to the corresponding experimental values observed by SEM. This comparison show good agreements between the corresponding results obtained by these two methods.

The experimental results obtained from microcracks in rock-like specimens show that the crack propagation mechanism may have the same trend as those specimens containing natural microcracks. The framework can be extended to the micromechanics of rocks and rock-like materials under various loading conditions (e.g., triaxial compressive, tensile and shear loading conditions).

Р е з ю м е

Скельні породи і скелеподібні матеріали часто руйнуються при стисненні внаслідок ініціювання, поширення і злиття мікротріщин, що з'явилися раніше. Виконано експериментальні і числові дослідження механізму процесу злиття мікротріщин у матеріалах типу скельних порід. Експериментальні дослідження включають випробування на одновісний стиск зразків, виготовлених із суміші цементу марки портланд пуцолан, слюди і води. Злиття мікротріщин вивчається на тонких зразках за допомогою скануючого електронного мікроскопа. Припускається, що вкраплення слюди відіграють роль мікротріщин у зразках. Також проведено деякі аналітичні і числові дослідження для моделювання явища злиття мікротріщин у зразках, що спостерігається експериментально. Для оцінки коефіцієнтів інтенсивності напружень по моді I і II у вершині мікротріщин використовується непрямий метод граничних елементів високого порядку, відомий як метод розриву переміщень високого порядку, що дозволяє використовувати спеціальні елементи в вершині тріщини для врахування сингулярності полів напружень і переміщень біля вершини тріщини. У програмі

розрахунку напружень використовується критерій руйнування по максимальних дотичних напруженнях у рамках лінійної механіки руйнування. При цьому поширення і злиття мікротріщин, розподілених у скельній породі за випадковим законом, оцінюється шляхом числового моделювання на основі ітеративного алгоритму. Отримані розрахункові результат порівнюються з відповідними експериментальними і числовими даними щодо злиття мікротріщин у скелеподібних матеріалах.

1. M. Bahaaddini, G. Sharrock, and B. K. Hebblewhite, "Numerical investigation of the effect of joint geometrical parameters on the mechanical properties of a non-persistent jointed rock mass under uniaxial compression," *Comput. Geotech*., **49**, 206–225 (2013).
2. L. N. Y. Wong and H. Q. Li, "Numerical study on coalescence of two pre-existing coplanar flaws in rock," *Int. J. Solids Struct.*, **50**, 3685–3706 (2013).
3. E. Mohtarami, A. Jafari, and M. Amini, "Stability analysis of slopes against combined circular-toppling failure," *Int. J. Rock Mech. Min. Sci.*, **67**, 43–56 (2014).
4. T. Funatsu, M. Kuruppu, and K. Matsui, "Effects of temperature and confining pressure on mixed mode (I–II) and mode II fracture toughness of Kimachi sandstone," *Int. J. Rock Mech. Min. Sci.*, **67**, 1–8 (2014).
5. R. L. Kranz, "Crack-crack and crack-pore interactions in stressed granite," *Int. J. Rock Mech. Min. Sci. Geomech. Abstr.*, **16**, 37–47 (1979).
6. C. A. Tang, P. Lin, R. H. C. Wong, and K. T. Chau, "Analysis of crack coalescence in rock-like materials containing three flaws – Part II: Numerical approach," *Int. J. Rock Mech. Min. Sci.*, **38**, 925–939 (2001).
7. M. Sagong and A. Bobet, "Coalescence of multiple flaws in a rock-model material in uniaxial compression," *Int. J. Rock Mech. Min. Sci.*, **39**, 229–241 (2002).
8. M. H. B. Nasseri and B. Mohanty, "Fracture toughness anisotropy in granitic rocks," *Int. J. Rock Mech. Min. Sci.*, **45**, 167–193 (2008).
9. A. Golshani, M. Oda, T. Takemura, and E. Munkhtogoo, "Numerical simulation of the excavation damaged zone around an opening in brittle rock," *Int. J. Rock Mech. Min. Sci.*, **44**, 835–845 (2006).
10. Y. Ichikawa, K. Kawamura, K. Uesugi, et al., "Micro- and macrobehavior of granitic rock: observations and viscoelastic homogenization analysis," *Comput. Meth. Appl. Mech. Eng.*, **191**, 47–72 (2001).
11. B. Obara, "Application of the image analysis method to the detection of transcrystalline microcracks observed in microscope images," *Arch. Min. Sci.*, **50**, 537–551 (2005).
12. M. F. Marji and E. Dehghani, "Kinked crack analysis by a hybridized boundary element/boundary collocation method," *Int. J. Solids Struct.*, **47**, 922–933 (2010).
13. M. F. Marji, "Numerical analysis of quasi-static crack branching in brittle solids by a modified displacement discontinuity method," *Int. J. Solids Struct.*, **51**, 1716–1736 (2014).
14. H. Horii and S. Nemat-Nasser, "Compression-induced microcrack growth in brittle solids: axial splitting and shear failure," *J. Geophys. Res.*, **90**, 3105–3125 (1985).
15. B. Shen, O. Stephansson, H. H. Einstein, and B. Ghahreman, "Coalescence of fractures under hear stress experiments," *J. Geoph. Res.*, **100**, 5975–5990 (1995).
16. A. Bobet, *Fracture Coalescence in Rock Materials: Experimental Observations and Numerical Predictions*, Sc.D. Thesis, Massachusetts Institute of Technology, Cambridge, USA (1997).

17. A. Bobet and H. H. Einstein, "Fracture coalescence in rock-type materials under uniaxial and biaxial compression," *Int. J. Rock Mech. Min. Sci.*, **35**, 863–888 (1998a).

18. J. Yoon, "Application of experimental design and optimization to PFC model calibration in uniaxial compression simulation," *Int. J. Rock Mech. Min. Sci.*, **44**, 871–889 (2007).

19. C. H. Park, *Coalescence of Frictional Fractures in Rock Materials*, Ph.D. Thesis, Purdue University, West Lafayette, Indiana (2008).

20. L. N. Y. Wong and H. H. Einstein, "Systematic evaluation of cracking behavior in specimens containing single flaws under uniaxial compression," *Int. J. Rock Mech. Min. Sci*., **46**, 239–249 (2009).

21. C. H. Park and A. Bobet, "Crack initiation and propagation from frictional fractures," in: Proc. of the 1st Canada-US Rock Mechanics Symposium (May 27–31, 2007, Vancouver, Canada) (2007), pp. 557–564.

22. C. H. Park and A. Bobet, "Crack coalescence in specimens with open and closed flaws: A comparison," *Int. J. Rock Mech. Min. Sci.*, **46**, 819–829 (2009).

23. C. H. Park and A. Bobet, "Crack initiation, propagation and coalescence from frictional flaws in uniaxial compression," *Eng. Fract. Mech.*, **77**, 2727–2748 (2010).

24. H. Lee and S. Jeon, "An experimental and numerical study of fracture coalescence in pre-cracked specimens under uniaxial compression," *Int. J. Solids Struct.*, **48**, 979–999 (2011).

25. P. Cheng-zhi and C. Ping, "Failure characteristics and its influencing factors of rock-like material with multi-fissures under uniaxial compression," *Trans. Nonferrous Met. Soc. China*, **22**, 185–191 (2012).

26. G. R. Irwin, "Analysis of stresses and strain near the end of crack traversing a plate," *J. Appl. Mech*., **24**, 361–364 (1957).

27. F. Erdogan and G. C. Sih, "On the crack extension in plates under loading and transverse shear," *J. Basic Eng.*, **85**, 519–527 (1963).

28. M. A. Hussian, E. L. Pu, and J. H. Underwood, "Strain energy release rate for a crack under combined mode I and mode II," in: *Fracture Analysis*, ASTM STP 560 (1974), pp. 2–28.

29. G. C. Sih, "Strain-energy-density factor applied to mixed mode crack problems," *Int. J. Fract.*, **10**, 305–321 (1974).

30. B. Shen and O. Stephansson, "Modification of the G-criterion for crack propagation subjected to compression," *Eng. Fract. Mech*., **47**, 177–189 (1994).

31. B. N. Whittaker, R. N. Singh, and G. Sun, *Rock Fracture Mechanics: Principles, Design and Applications. Developments in Geotechnical Engineering*, Elsevier, Amsterdam (1992).

32. L. F. Vesga, L. E. Vallejo, and S. Lobo-Guerrero, "DEM analysis of the crack propagation in brittle clays under uniaxial compression tests," *Int. J. Num. Anal. Meth. Geomech.*, **32**, 1405–1415 (2008).

33. F. Ouchterlony (ISRM Commission on Testing Methods), "Suggested methods for determining the fracture toughness of rock," *Int. J. Rock Mech. Min. Sci. Geomech. Abstr*., **25**, 71–97 (1988).

34. R. J. Fowell (ISRM Commission on Testing Methods), "Suggested method for determining mode I fracture toughness using cracked chevron notched Brazilian disc (CCNBD) specimens," *Int. J. Rock Mech. Min. Sci. Geomech. Abstr.*, **32**, 57–64 (1995).

35. H. Guo, N. I. Aziz, and R. A. Schmidt, "Linear elastic crack tip modeling by displacement discontinuity method," *Eng. Fract. Mech*., **36**, 933–943 (1990).

36. H. Guo, N. I. Aziz, and R. A. Schmidt, "Rock cutting study using linear elastic fracture mechanics," *Eng. Fract. Mech.*, **41**, 771–778 (1992).

37. C. Scavia, "Fracture mechanics approach to stability analysis of crack slopes," *Eng. Fract. Mech*., **35**, 889–910 (1990).

38. M. H. Aliabadi and D. P. Rooke, *Numerical Fracture Mechanics*, Computational Mechanics Publications, Southampton, UK (1991).

39. M. H. Aliabadi, *Fracture of Rocks*, Computational Mechanics Publications, Southampton, UK (1998).

40. H. Haeri, K. Shahriar, M. F. Marji, and P. Moarefvand, "On the strength and crack propagation process of the pre-cracked rock-like specimens under uniaxial compression," *Strength Mater*., **46**, No. 1, 140–152 (2014).

41. R. J. Sanford, *Principles of Fracture Mechanics*, Pearson Education, Upper Saddle River, New Jersey (2003), pp. 1–15.

Received 22. 09. 2014